JOURNAL OF CATALYSIS 99, 293–303 (1986)

Electronic Effect of Supports on Copper Catalysts

HSIU-WEI CHEN,* J. M. WHITE,* AND J. G. EKERDT†

*Department of Chemistry and †Department of Chemical Engineering, The University of Texas at Austin, Austin, Texas 78712

Received July 30, 1985; revised January 3, 1986

The adsorption and hydrogenation properties of various semiconductor-supported copper catalysts were studied and are interpreted in terms of the electronic properties of the semiconductor. Electronic interactions between copper and *p*-type ZrO_2 and Cr_2O_3 enhance the quantity and stability of CO adsorption on copper and increase by a factor of 10 to 20 the activity for CO hydrogenation as compared with bulk copper. Infrared spectra and XPS results suggest that high-temperature reduction (500°C) of Cr_2O_3 (producing an *n*-type material) may produce some lower oxidation state Cr ions and destroy the promoting effect of Cr_2O_3 on copper. Copper on insulator (Al_2O_3 and SiO_2) and *n*-type (ZnO and C) supports all have about the same CO hydrogenation activity as pure copper, while TiO_2- and MgO-supported Cu (*n*-type) have barely detectable activity.

INTRODUCTION

The materials used to support metal catalysts not only provide large surface areas for dispersion of the metals, but can also affect the gas adsorption and activity/selectivity of the supported metals. One of the important support effects which has attracted considerable attention recently is the strong metal–support interaction (SMSI) (*1–3*). Group VIII-B metal/titania systems are typical SMSI catalysts. One characteristic of SMSI is the suppression of H_2, CO, and NO (*4*) chemisorption. Many TiO_2-supported metal catalysts also have higher methanation activities than their corresponding Al_2O_3-supported counterparts (*5–7*).

Several physical and chemical effects, including encapsulation (*8–11*), electronic interaction (*12–15*), diffusion (*16*), and morphology modification (*17*), have been suggested as contributors to the SMSI effect. As applied to titania–Group VIII metal systems, the electronic interaction model suggests that the SMSI effect involves a redistribution of the conduction band electron density from partially reduced titania to the supported metal particles. While charge transfer to or from the metal may occur at the interface, it is not possible to transfer enough charge to alter significantly the oxidation state of all of the atoms, even in a small metal particle. The electric field can not be sustained; any charge that is transferred across the interface will be completely screened over a distance of roughly one lattice spacing. Furthermore, the small concentration of conduction band electrons in a typical semiconductor makes extensive transfer to the metal even more improbable. However, charge redistribution (rehybridization) can occur over much larger distances and does not require any net transfer (*41*). Thus, a small amount of charge transfer (or even an interaction with no net local charge transfer) at a metal–support interface can alter the *s*-, *p*-, *d*-character of the charge distribution several (at least 3 or 4) atomic spacings away. Alteration of the electron density and state distribution of the metal may give a material which has altered chemisorption and catalytic properties. Even if most of the metal atoms behave as if the support were absent, the interface must be considered and metal atoms located there may be strongly altered by interactions with

0021-9517/86 $3.00

the support (with or without charge transfer). For small metal particles and encapsulated large metal particles, the fraction of these interface atoms can be large and have a major influence on catalytic reactions (*6, 37*).

If this mechanism is indeed operative in SMSI, then it should also be possible to change the direction and extent of electronic charge redistribution and thereby activate relatively inactive metals for the adsorption of hydrogen (i.e., invert the normal SMSI effect). In this paper we address this question by using a relatively inactive metal, Cu, and a variety of supports with different electronic properties (discussed below). These materials were investigated for CO and H_2 chemisorption and for CO hydrogenation activity.

The goal is to *increase* the chemisorption of CO and H_2 and to alter the CO hydrogenation activity over the supported metal. From the point of view of the electronic interaction model, we are trying either to redistribute some electron density in the transition metal atoms by virtue of interactions at the metal–support interface or to withdraw some electron density from the metal to the support (or into oxide particles that decorate the surface of the metal). Some results from the literature suggest that redistributing electron density between the group IB metals and the group VIIIB metals is one factor in altering catalytic activity for certain reactions. As an example, Ni–Cu alloys have about one order higher activity for ethylene hydrogenation than pure Ni (*22*). On the other hand, Ni–Au alloys have about one-tenth the reactivity of pure Ni (*22*). The work functions of Ni, Cu, and Au are 5.06, 4.55, and 5.32 eV, respectively (*23*). Thus, electron density transfer from Cu to Ni is expected in a Ni–Cu alloy but from Ni to Au in a Ni–Au alloy. As a second example, the activity of the Pt–Au system for the cyclohexane dehydrogenation reaction was 6 times higher than with pure Pt (*24*). The work functions of Pt and Au are 5.42 and 5.32 eV, respectively (*23*). Similar conclusions have been drawn for chemisorption on single crystal Ru(0001) covered with Cu (the work function of Ru exceeds that of Cu). Copper overlayers up to at least two layers thick is more active for O_2 chemisorption than bulk Cu (*40*) and CO chemisorption on Cu is thermally more stable when the Cu overlayer is on Ru than when it is on Cu (*39*).

Of course, other factors such as geometry and lattice effects may also contribute to the activity behavior. In the context of the present discussion, it is important to appreciate the indirect role that electronic interactions can have on the structure of metal particles. In any case where the metal–substrate interaction is a significant fraction of the metal–metal interaction, we expect changes in metal–metal internuclear distance in the first layer. In turn higher layers will have structures "guided" by the first layer. These include growth modes and distribution of exposed crystal faces.

With electronic interaction model in mind, we establish the following conditions for the selection of metal and support combinations to provide an *inverse* of the normal SMSI effect.

For the support. The support should have some electron conductivity and a higher work function than the supported metal so that the support can accept the electron density from the metal. The support should also have enough surface area to disperse the supported metals.

For the metals. The metal should have a lower work function than the support, should show weak adsorption of CO and H_2 in its normal state and should have weak hydrogenation activity so that increases can be observed easily.

Among the group IB metals, copper is the best candidate because it has weak hydrogenation activity (*25*), weak adsorption of CO and H_2 (*26*), and relatively low work function (4.55 eV) (*23*). ZrO_2 and Cr_2O_3 are *p*-type semiconductors with higher work functions than copper. These oxides were used as supports in the experiments out-

lined below. Some insulator (Al_2O_3, SiO_2) and *n*-type semiconductors with higher or lower work functions than copper (graphite, ZnO, TiO_2, and MgO) were also used as references. The results are generally consistent with electronic interaction model but, recognizing the complexity of SMSI effects, we cannot go beyond a consistency argument.

EXPERIMENTAL

The supports used in this study were ZrO_2 (Baddeleyite-type, 99+% pure, Alfa-Ventron Co., 5.5 m^2/g), Cr_2O_3 (Fisher Co. certified grade, 11 m^2/g), graphite (Alfa-Ventron Co., 9 m^2/g), ZnO (The New Jersey Zinc Co., Kadox-15, 7.8 m^2/g), Al_2O_3 (MCB Inc. chromatographic grade, type F-20, 80–200 mesh, 258 m^2/g), SiO_2 (Cab-O-sil HS-5, 325 m^2/g), TiO_2 (MCB Inc., 75% anatase and 25% rutile, 10 m^2/g), and MgO (Fisher Co. certified grade, 30 m^2/g).

The catalysts were prepared by impregnating the supports with an aqueous solution of $Cu(NO_3)_2 \cdot 3H_2O$ (MCB Ind., reagent grade). The resulting catalysts were dried at 100°C and calcined in air at 200°C for 16 h.

UHP hydrogen (Big Three Industrial, Inc.) was further purified by passing it through a deoxo purifier (Matheson Corp.). CO (contaminated with 200 ppm C_1 and 10 ppm C_2 of hydrocarbons, Big Three Industrial Inc.) was passed through a molecular sieve trap at 125°C to remove any carbonyls. N_2O (Matheson Corp.) was purified by a freeze–thaw technique. Oxygen (Big Three Industrial, Inc.) was used without any further purification.

Adsorption measurements were made with a typical glass volumetric adsorption system capable of a dynamic vacuum of $\leqq 10^{-5}$ Torr. Approximately 0.2 g of the catalyst was placed in a glass adsorption cell and reduced by H_2 *in situ* at 275°C (or otherwise specified in the text). The sample was outgassed under vacuum ($\leqq 10^{-4}$ Torr) at 400°C for 30 min before the uptake experiment. The pressure was recorded every 5 min during the adsorption process until the pressure change was less than 0.01 Torr in 5 min.

The average crystallite size of the supported copper was estimated from the (111) line of copper by the X-ray line broadening method. The number of surface copper atoms was determined from the N_2 pressure which was produced by decomposition of N_2O (*18, 19*):

$$N_2O + 2\,Cu \longrightarrow Cu_2O + N_2$$

For this procedure, approximately 0.5 g of the catalyst was placed in the reaction cell, reduced in flowing hydrogen at the temperature of interest for 6 h, degassed at the same temperature for 30 min and cooled to room temperature under vacuum. Then 200 Torr of N_2O was dosed into the cell at room temperature to react with the copper for 5 h. The unreacted N_2O was trapped into a side tube cooled to liquid-nitrogen temperature, and the resulting N_2 pressure was measured with a pressure transducer (MKS Baratron). The residual N_2O pressure at liquid-nitrogen temperature was undetectable with this pressure sensor.

For IR measurements, 50–100 mg catalyst was spread uniformly on paraffin paper and pressed at 4000 psi to make a 1-in.-diameter wafer. The resulting wafer was heated under vacuum at 400°C for 1 h, oxidized in 1 atm O_2 at 225°C for 6 h, degassed at the same temperature for 1 h, reduced at 275°C in 1 atm H_2 for 16 h, and degassed at 400°C for 1 h before IR measurement. The standard IR cell has been described (*20*). Spectra were taken using a Nicolet 7199 FT-IR spectrometer and were recorded at room temperature with resolution of 2 cm^{-1}. All spectra reported here have been corrected by subtraction for absorption by the gas phase, blank catalyst wafer, and CaF_2 windows.

The CO hydrogenation was carried out in a quartz fixed-bed reactor operating in a differential mode at low conversion. The reaction system is shown in Fig. 1. Samples of 1 to 7 g were pretreated *in situ* in flowing H_2

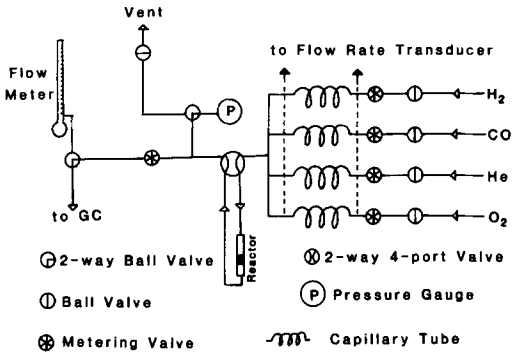

FIG. 1. The CO hydrogenation reactor system.

(~15 cm^3/min) at 280°C for 6 h. The reaction temperature ranged from 250 to 275°C. The CO/H_2 ratio was 1 : 3 and the total pressure was 1 atm. Space velocities varied from 2500 to 5000 h^{-1} to achieve a differential conversion of CO. The H_2/CO feed stream passed over the catalyst for 10 min before a sample was taken for analysis. The catalyst was purged with H_2 for 30 min between each H_2/CO exposure to maintain the catalytic activity. The procedure was similar to that used by Sinfelt (*21*). A Varian 3700 gas chromatograph was used to analyze the products with a 20% OV-101 on a Chromosorb P-AW column. Product gas concentrations were determined with a Hewlett–Packard 3390A integrator by comparing the product peak areas to those for a standard mixture. The turnover number was calculated as

$$n = A\frac{cf}{N},$$

where

n = turnover number (molecules of CO consumed to produce hydrocarbon per second per surface Cu atom);

c = CO consumption on 1 g of catalyst in units of ppm of total gas (corrected for conversion on 1 g of blank support);

f = flow rate, cm^3/min;

N = number of surface copper atoms per gram of catalyst determined by N_2O decomposition method; and

A = constant to convert the units from (ml × ppm)/(atom × min) to (molecule)/(atom × s).

The CO consumption was calculated from the product hydrocarbons. Oxygenated compounds were not detected in sufficient concentrations under our experiments to be included in the turnover number calculation. This may be due in part to the chromatographic column used.

The catalyst surface composition was determined by X-ray photoelectron spectroscopy (XPS) in a VG ESCALAB system. The sample pretreatment method was the same as for the CO hydrogenation experiment. The powder was spread onto a sample holder and put into the entry chamber and reduced again *in situ* in 5 Torr H_2 275°C for 1 h. The XPS spectra was taken using MgKα ($h\mu$ = 1253.6 eV) radiation. The position of the C(1*s*) line (284.5 eV binding energy, BE) was used to estimate sample charging.

RESULTS AND DISCUSSION

(*A*) *CO Hydrogenation*

Table 1 summarizes the properties of the supported copper catalysts. The turnover number of CO on SiO_2-supported copper was about 0.02×10^{-3} which is consistent with Vannice's results (*28*).

There are significant differences in CO hydrogenation for the nine different Cu-based catalysts. These fall into three classes: (1) larger than bulk Cu; (2) about the same as bulk Cu; and (3) less than bulk Cu.

Many things can affect the activity of the supported Cu. However, as discussed below, particle size, crystal orientation, the intrinsic activity of the support itself, and the extent of copper reduction are not solely responsible for the differences. All the catalysts listed in Table 1, except bulk Cu, have roughly the same particle size (Table 2). Copper(111) XRD lines of nearly the same width dominate the spectra of every sample suggesting that the particle

TABLE 1

Properties of Supported Cu Catalysts (CO Hydrogenation Activity)

Sample	ϕ^a	Surface Cu (%) Total Cu	TON[b] ($\times 10^{+3}$)	Conductivity type[c] of the support
5% Cu/ZrO_2	5.0	0.6	0.41(0.68) ± 0.05	*p*
5% Cu/Cr_2O_3	5.8	1.0	0.24(0.27) ± 0.02	*p*
5% Cu/graphite	4.8	1.0	≤0.04(0.05)	*n* (semimetal)
5% Cu/ZnO	4.6	0.6	≤0.03	*n*
20% Cu/Al_2O_3	—	1.6	≤0.01(0.03)	Insulator
20% Cu/SiO_2	—	0.3	≤0.02	Insulator
5% Cu/TiO_2	3.0	0.5	≤0.01	*n*
5% Cu/MgO	3.5	—	≤0.01	*n*
Cu(bulk)	4.55	0.0029	≤0.02	Metal

[a] Work function of the support (*27*).

[b] Turnover number of CO × 10^{+3}, the number in parentheses is the measured TON before subtracting the activity of the blank support. The unit is molecules of CO/atoms of surface Cu, per second. H_2/CO =3, flow rate = 60 cm^3/min, total pressure = 1 atm, T = 275°C.

[c] From Ref. (*27*).

size and the crystal orientation have little effect on CO hydrogenation activity. Blank Al_2O_3 has about the same activity as blank ZrO_2 (on the basis of the weight of oxides) but the former has no promotion effect on Cu so that the effect of the intrinsic CO hydrogenation activity of the support itself was ruled out. There is no relationship between the specific activity (TON of CO) and the extent of copper prereduction (discussed in the XPS section).

We propose that the cause of the variation in CO hydrogenation activity is largely electronic in origin and involves the *interfaces* between Cu particles and the supports: for Cu supported Cr_2O_3 or ZrO_2, *p*-type semiconductors with work functions higher than Cu, the CO hydrogenation activity is higher than with bulk Cu. Electron density can transfer from Cu to the support in this case. When Cu is supported on SiO_2 or Al_2O_3, both insulators, the activity is about the same as with bulk Cu. Electron density cannot be accepted by these insulators. Copper-supported *n*-type semiconductors with work functions higher than Cu also have roughly the same activity as bulk Cu.

TABLE 2

Particle Size and Infrared Spectra of Adsorbed CO

Sample	Particle size[a] (Å)	P_{CO} (Torr)	ϕ^b	IR peak area		Area ratio after/before evacuation
				Before evac.	After evac.	
Cu/Cr_2O_3	290	20	5.8	378(2116)[c]	138(2111)	0.36 ± 0.07
Cu/ZrO_2	390	18	5.0	259(2128)	89 (2128)	0.34 ± 0.07
Cu/SiO_2	390	18	—	200(2127)	28 (2126)	0.14 ± 0.03
Cu/TiO_2	340	20	3.0	128(2131)	13 (2131)	0.10 ± 0.02

[a] By X-ray line broadening method.

[b] Work function of support in eV.

[c] In parentheses is the IR peak position, cm^{-1}.

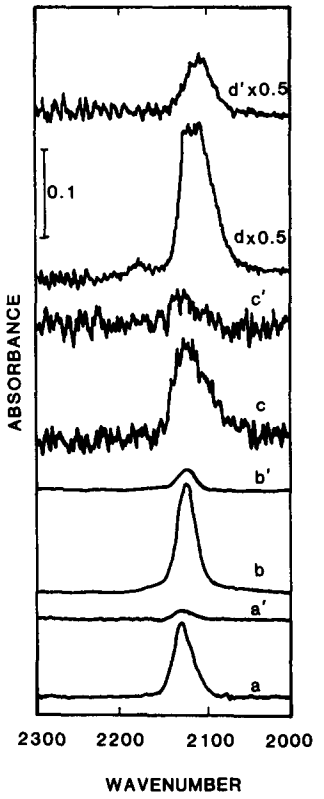

FIG. 2. CO adsorption at room temperature on copper catalysts reduced at 225°C. (a) 20 Torr CO on Cu/SiO_2, (a') evacuate for 10 min, (b) 18 Torr CO on Cu/TiO_2, (b') evacuate for 10 min, (c) 18 Torr CO on Cu/ZrO_2, (c') evacuate for 10 min, (d) 20 Torr CO on Cu/Cr_2O_3, (d') evacuate for 10 min.

Charge transfer from the metal to the *n*-type semiconductor may not occur even when the work function of the metal is less than the work function of the semiconductor (*29, 30*). Significant transfer will occur only when the conduction band electron density is lower than the density at the boundary between the metal and the semiconductor. On the basis of the treatment given in reference (*29*), we expect there will be no charge transfer from Cu to ZnO. Although the calculation is not very accurate because the surface properties of powdered semiconductors are not well understood, ZnO is not expected to promote the activity of CO hydrogenation on Cu (on the basis of the electronic interaction model).

An interesting case is Cr_2O_3, which switches from *p*-type to *n*-type upon reduction. The *p*-type material promotes Cu but *n*-type does not (see below). Copper supported on TiO_2 or MgO (*n*-type semiconductors with work functions lower than Cu) have activity less than bulk Cu. These results are what we would expect from the model proposed above.

(B) CO and H_2 Adsorption

Encouraged by the results of the CO hydrogenation reaction, we investigated the adsorption behavior of the catalysts. Some of the supports adsorb carbon monoxide, and it is difficult to distinguish the CO adsorbed on the metal and support by conventional volumetric methods. Infrared spectra are helpful in locating the CO. The position of the band of adsorbed CO on copper is between 2100 and 2130 cm^{-1} while on oxide supports it is between 2150 and 2200 cm^{-1}.

The IR results for CO adsorption on Cr_2O_3-, ZrO_2-, TiO_2-, and SiO_2-supported Cu are shown in Fig. 2 and summarized in Table 2. The area ratio (Table 2) of the IR bands after and before evacuation for 10 min at room temperature provides one measure of strongly and weakly held CO (ignoring variations of absorption cross section). On Cr_2O_3- and ZrO_2-supported Cu the stability of adsorbed CO is higher than on SiO_2 or TiO_2-supported Cu. Assuming that insulator-supported Cu (Cu/Al_2O_3 or Cu/SiO_2) has the same metal properties as bulk Cu, then they can be used as standards against which to compare the other supports. SiO_2 is better because Cu/SiO_2 has roughly the same hydrogenation activity as pure Cu powder (see Table 1). Compared with Cu/SiO_2, the quantity and stability of adsorbed CO on the other catalysts correlates with the bulk electronic character of the support (Table 2). *p*-Type semiconductors with work functions higher than that of bulk Cu show more extensive and more stable CO adsorption than Cu/SiO_2. Titanium dioxide is an *n*-type semiconductor and has a lower work function than Cu. Carbon monoxide

adsorbed on TiO_2-supported Cu is not significantly different from CO on SiO_2-supported copper. In the context of this discussion, it is more important to note that connections between the chemisorbed CO (as detected by IR) and catalytic activity have not been established for Pt on a variety of supports (*38*). Thus, the correlation observed here must not be taken as generalizable.

When the CO band lies between 2110 and 2140 cm^{-1} it has been assigned to adsorption on poorly reduced Cu (*31*). As the energies of the CO bands on all the catalysts in Table 2 were higher than 2110 cm^{-1}, one might argue that the variation in the stability of CO was due to oxidized Cu. However, our XPS results suggest that the CO hydrogenation activity and the chemisorption stability of CO on Cu/semiconductor catalyst are not directly related to the oxidation state of Cu. This will be discussed in the XPS section.

Qualitatively, hydrogen adsorption shows the same trend as CO on these Cu catalysts. Unfortunately, the quantity of the adsorbed H_2 was very small (<2 μmol/g), so quantitative comparisons were not possible. The very weak chemisorption of hydrogen on clean copper films is known (*32*).

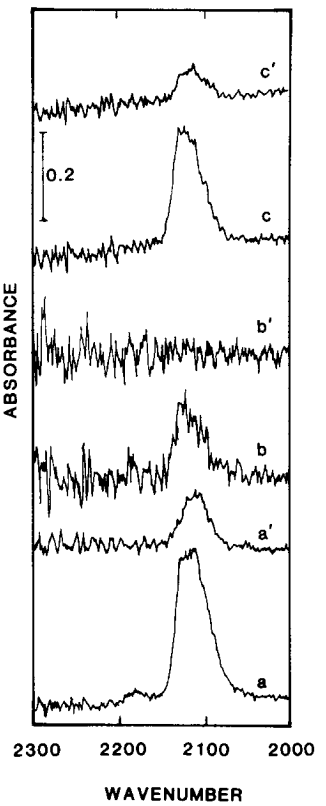

FIG. 3. CO adsorption at room temperature on various reduced Cu/Cr_2O_3 catalysts. (a) 24 Torr CO on Cu/Cr_2O_3 reduced at 225°C, (a') evacuate for 10 min, (b) 26 Torr CO on Cu/Cr_2O_3 reduced at 500°C, (b') evacuate for 10 min, (c) 22 Torr CO on (b') after it was oxidized and reduced at 225·C, (c') evacuate for 10 min.

(C) *Reducibility of Cr_2O_3 and Its Electronic Effect*

The formal valence state of chromium varies from 0 to +6 in known compounds and different valence state chromium species might exist on a chromia surface treated with hydrogen since Cr_2O_3 is a reducible oxide (*2*). The electronic properties of chromia are very dependent on the extent of reduction of its surface. The mechanism of the conductivity of Cr_2O_3 changes from hole conduction type (*p*-type) to electron conduction type (*n*-type) after high-temperature reduction (*33*). Thus it is of interest to examine the effect of reduction temperature on the Cr_2O_3-supported copper. Figure 3 shows the CO adsorption on reduced Cu/Cr_2O_3. After a low-temperature (225°C) reduction, 36% of CO can be held on the copper surface after evacuation to 10^{-4} Torr at room temperature for 1 min (Fig. 3a'). After a high temperature (500°C) reduction, no adsorbed CO was observable under the same conditions as those in Fig. 3a' (Fig. 3b'). Oxidation followed by low-temperature reduction restores the ability to hold the adsorbed CO strongly (Fig. 3c'). This kind of behavior is like that of prototype SMSI catalysts (e.g., Pt/TiO_2).

Previous literature reports that Cr_2O_3-supported Pt shows no SMSI effect (*2*). Within the framework of our model this occurs because of the difference in electron conduction behavior of Cr_2O_3 and TiO_2.

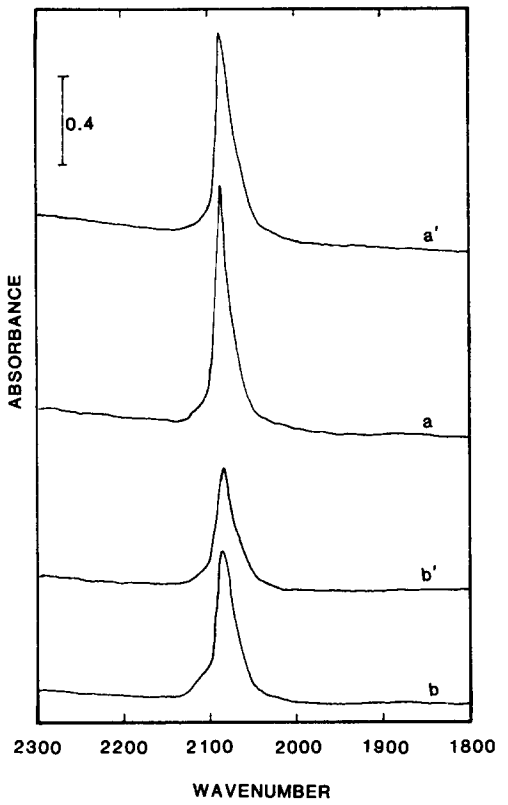

FIG. 4. CO adsorption at room temperature on various reduced Pt/Cr_2O_3 samples. (a) 16 Torr CO on Pt/Cr_2O_3 reduced at 225°C, (a') evacuate for 10 min, (b) 16 Torr CO on Pt/Cr_2O_3 reduced at 500°C, (b') evacuate for 10 min.

TiO_2 is an *n*-type semiconductor and has a lower work function than Pt while Cr_2O_3 is a *p*-type semiconductor and has a higher work function than Pt. We have repeated CO adsorption experiments on the Pt/Cr_2O_3 system (Fig. 4) and confirm that there is no suppression of CO chemisorption that could be taken as evidence for a significant metal–support interaction. The band area ratios are almost the same (84 and 81%) for the low and high temperature reduction of Pt/Cr_2O_3.

An *inverse* of the typical SMSI type electronic effect is proposed for our Cu/Cr_2O_3 system: reduction at 225°C does not produce a *n*-type semiconductor surface, and electron density can be shifted from Cu to the support. The result is an interaction (which could include encapsulation of the Cu) that leads to a higher binding energy of CO on Cu/Cr_2O_3 than on metallic Cu. High-temperature (500°C) reduction produces some lower valence state chromium ions on the Cr_2O_3 surface and changes the mechanism of conductivity from *p*-type to *n*-type. This electron-rich surface destroys the inverse SMSI state and the Cu/Cr_2O_3 should behave as normal copper under this condition (i.e., very weakly held CO). Oxidation removes the low-valence-state chromium ions produced by high-temperature reduction. A subsequent 225°C reduction reduces the surface copper oxide but leaves chromia as a *p*-type material. Thus, its electron accepting ability is restored and the inverse SMSI effect reappears.

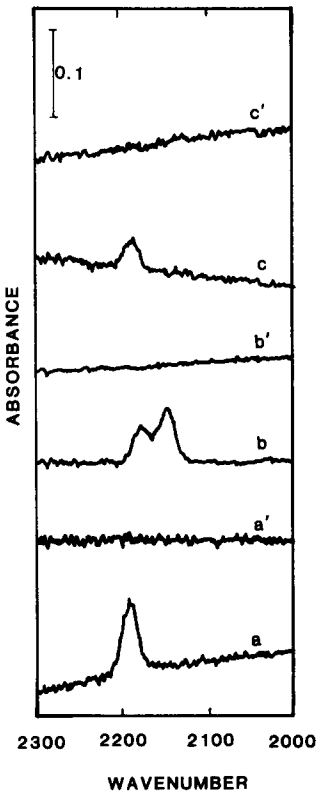

FIG. 5. CO adsorption at room temperature on various reduced Cr_2O_3 substrates. (a) 22 Torr CO on Cr_2O_3 reduced at 225°C, (a') evacuate for 10 min, (b) 24 Torr CO on Cr_2O_3 reduced at 500°C, (b') evacuate for 10 min, (c) 22 Torr CO on (b') after it was oxidized and reduced at 225°C, and (c') evacuate for 10 min.

TABLE 3

XPS Analysis of Copper–Chromia Catalysts

Temp.[a]	Binding energy, eV (FWHM)			Peak area ratio[b]		
	O(1*s*)	Cr($2p_{3/2}$)	Cr($2p_{3/2}$)	Cu/Cr	Cu/O	Cr/O
275°C	530.3(2.7)[c]	576.7(3.9)	932.7(3.5)	0.31	0.10	0.32
500°C	530.3(2.6)	576.6(3.9)	932.6(3.7)	0.19	0.07	0.37

[a] The reduction temperature of Cu/Cr_2O_3.
[b] The deviation is about 15%.
[c] Binding energies in eV with full width at half maximum in parentheses.

IR of CO adsorption on blank Cr_2O_3 (no Cu) provides some evidence that the surface electron density on Cr_2O_3 reduced at 500°C is higher than when it was reduced at 225°C. Figure 5 shows the CO adsorption data. CO is reversibly adsorbed on Cr_2O_3 (no Cu) at room temperature for every sample. The frequency of CO on 225°C reduced Cr_2O_3 is at 2191 cm^{-1}. It shifts downward and splits into two bands at 2179 and 2150 cm^{-1} after a 500°C reduction. This lower frequency CO band is consistent with a higher electron concentration on 500°C reduced Cr_2O_3 than that on the 225°C reduced surface. This extra electron concentration increases the back bonding strength between the oxide and the π^* orbital of CO which would produce the observed lower frequency band.

(D) XPS Study

Table 3 shows the XPS data for Cu/Cr_2O_3 reduced at 275 and 500°C. The binding energies of Cr and Cu after reduction at 275°C were about 0.1 eV higher than after a 500°C reduction. The complexity of the powder sample environment makes it difficult to interpret this binding energy shift (changes in final state relaxation can not be readily addressed). However, the observations are not inconsistent with the notion that small amounts of charge transfer from Cu to Cr_2O_3 occur when the latter is reduced at relative low temperature and that this capacity is lost when chromia is reduced at high temperatures. The increase of the Cr-derived XPS binding energy upon high-temperature reduction can be understood in terms of the loss of oxygen from the surface during reduction.

The areas of the Cu, O, and Cr XPS peaks also provide some information about the surface composition. The ratio of Cu/Cr and Cu/O decreases as the reduction temperature increases, suggesting that Cu was sintered under high-temperature reduction. This is consistent with the X-ray line broadening data and the reduced infrared band intensity of CO adsorption in Fig. 3. The ratio of Cr/O increases about 20% after high-temperature reduction, suggesting that the surface chromium should be in a lower oxidation state (the broad XPS peak from the powder sample prevents resolution of different Cr states). This is consistent with the IR results for CO adsorption on Cr_2O_3 (Fig. 5).

The extent of copper reduction on various oxide supports was also examined using the Auger parameter (see Table 4) (*34*, *35*). When the Auger parameter is in the 1851-eV region and no satellite appears beside the Cu($2p_{3/2}$) XPS peak, Cu^0 is the dominant valence state. When a satellite appears beside the Cu($2p_{3/2}$) XPS peak, Cu^{2+} is dominant. The percentage of Cu^+ was determined by the peak height of the X-ray excited Auger line Cu^+ (916.6 eV) and Cu^0 (918.6 eV) when there was no Cu^{2+} on the surface (Cu^{2+} also shows an Auger signal near 918.6 eV). The Cu^+ content on Cu/ZrO_2 is difficult to determine because of

TABLE 4

Auger Parameter Results

Sample	Auger parameter (Cu)	$Cu^+/Ci^+ + Cu^0$ (%)
Cu	1851.2	—
Cu/Cr_2O_3	1851.5	≤5
Cu/Cr_2O_3[a]	1851.5	≤5
Cu/ZrO_2	1851.2	—[b]
Cu/SiO_2	1851.2	≤5
Cu/Al_2O_3	1851.3	14 ± 5
Cu/TiO_2	1849.4	50 ± 10

[a] Reduced at 500°C, the other are reduced at 275°C.
[b] Overlap with $Zr(3p_{1/2})$ XPS peak.

the overlap of the Auger peak and $Zr(3p_{1/2}$ XPS peak.

Comparing the Cu^+ content (Table 4) with the catalyst activity (Table 1), we conclude that the CO hydrogenation activity cannot be explained solely on the basis of the Cu^+ content. We suspect that the active sites involve the combination of Cu^0 and a copper species with electronic structure between Cu^0 and Cu^+ which is induced by the electronic influence of the support (i.e., interface sites (*6, 37*)). The high Cu^+ content (50%) on Cu/TiO_2 might be the result of the interdiffusion and reaction between Cu and TiO_2 (*36*).

CONCLUSIONS

From the CO hydrogenation activity, the CO adsorption and stability, and the XPS data, we conclude that Cu–support interactions of significance are detectable. A *p*-type semiconductor with a work function higher than Cu, such as ZrO_2 and Cr_2O_3, can promote rather than inhibit CO adsorption. The rate of CO hydrogenation is also increased. The *n*-type semiconductors have little or no promotion effect on CO adsorption and hydrogenation activity. These results are interpreted in terms of electronic interactions between the supports and copper. The local and longer range character of various kinds of electronic interactions are discussed. Extensive charge transfer is not required to alter the chemical character of metal particles on supports. Metal particle size and the activity of the support itself are not responsible for the variations of the CO adsorption and hydrogenation on these Cu catalysts. High-temperature reduction of Cu/Cr_2O_3 produces some lower oxidation state sites on the Cr_2O_3 surface. We propose that these inhibit electron density transfer from Cu to Cr_2O_3 and decrease the chemisorption of CO. Oxidation followed by low-temperature reduction restores the chemisorption state.

ACKNOWLEDGMENTS

This research was supported in part by the Office of Naval Research (J. M. W.) and by the National Science Foundation, CPE-831994 (J.G.E.).

REFERENCES

1. Tauster, S. J., and Fung, S. C., *J. Catal.* **55,** 29 (1978).
2. Tauster, S. J., Fung, S. C., Baker, R. T. K., and Horsley, J. A., *Science* **211,** 1121 (1981).
3. Baker, R. T. K., Prestridge, E. B., and McVicker, G. B., *J. Catal.* **89,** 422 (1984).
4. Fang, S.-M., and White, J. M., *J. Catal.* **83,** 1 (1983).
5. Vannice, M. A., *J. Catal.* **74,** 199 (1982).
6. Burch, R., and Flambard, A. R., *J. Catal.* **76,** 389 (1982).
7. Ching, Y.-W., Xiong, G., and Kao, C.-C., *J. Catal.* **85,** 237 (1984).
8. Santos, J., Phillips, J., and Dumesic, J. A., *J. Catal.* **81,** 147 (1983).
9. Belton, D. N., Sun, Y.-M., and White, J. M., *J. Amer. Chem. Soc.* **106,** 3059 (1984).
10. Belton, D. N., Sun, Y.-M., and White, J. M., *J. Phys. Chem.* **88,** 5172 (1984).

11. Sadeghi, H. R., and Henrich, V. E., *J. Catal.* **87,** 279 (1984).
12. Chen, B.-H., and White, J. M., *J. Phys. Chem.* **86,** 3534 (1982).
13. Horsley, J. A., *J. Amer. Chem. Soc.* **101,** 2870 (1979).
14. Chien, S. H., Shelimov, B. N., Resasco, D. E., Lee, E. H., and Haller, G. L., *J. Catal.* **77,** 301 (1982).
15. Sexton, B. A., Hughes, A. E., and Foger, K., *J. Catal.* **77,** 85 (1982).
16. Ko, C. S., and Gorte, R. J., *J. Catal.* **90,** 59 (1984).
17. Baker, R. T. K., Prestridge, E. C., and Garten, R. L., *J. Catal.* **56,** 390 (1979).
18. Dell, R. M., Stone, F. S., and Tiley, P. F., *Trans. Faraday Soc.* **49,** 195 (1953).
19. Scholten, J. J. F., and Konvalinka, J. A., *Trans. Faraday Soc.* **65,** 2465 (1969).
20. Tanaka, K., and White, J. M., *J. Catal.* **86,** 4708 (1982).
21. Sinfelt, J. H., *Chem. Eng. Sci.* **23,** 1181 (1968).
22. Campbell, J. S., and Emmett, P. H., *J. Catal.* **7,** 252 (1967).
23. Anderson, J. R., "Structure of Metallic Catalysts." Academic Press, New York, 1975.
24. Sachtler, J. W. A., Biberian, J. P., and Somorjai, G. A., *Surf. Sci.* **110,** 43 (1981).
25. Khulbe, K. C., Mann, R. S., and Manvogian, A., *Chem. Rev.* **80,** 417 (1980).
26. Bond, G. C., "Heterogeneous Catalysis: Principles and Applications." Ox Oxford Univ. Press, 1974. London/New York.
27. Krylov, O. V., "Catalysis by Nonmetals." Academic Press, New York, 1970.
28. Vannice, M. A., *J. Catal.* **50,** 228 (1977).
29. Baddour, R. F., and Deibert, M. C., *J. Phys. Chem.* **70,** 2173 (1966).
30. Spenke, E., "Electronic Semiconductor." McGraw–Hill, New York, 1958.
31. Pritchard, J., Catterick, T., and Gupta, R. K., *Surf. Sci.* **53,** 1 (1975).
32. Alexander, C. S., and Pritchard, J., *J. Chem. Soc. Faraday Trans. 1* **68,** 202 (1972).
33. Chaplin, R., Chapman, P. R., and Griffith, R. H., *Nature (London)* **172,** 77 (1953).
34. Fleisch, T. H., and Mains, G. J., *Appl. Surf. Sci.* **10,** 51 (1982).
35. Apai, G. R., Monnier, J. R., and Hanrahan, M. J., *J. Chem. Soc., Chem. Commun.*, 212 (1984).
36. Belton, D. N.,, Ph. D. dissertation. Univ. of Texas, Austin, Texas, 1985.
37. Vannice, M. A., and Sudhakar, C., *J. Phys. Chem.* **88,** 2429 (1984).
38. Vannice, M. A., Turu, C. C., and Moon, S. H., *J. Catal.* **79,** 70 (1983).
39. Houston, J. E., Peden, C. F. H., Blair, D. S., and Goodman, D. W., private communication.
40. Shi, S.-K., Lee, H.-I., and White, J. M., *Surf. Sci.* **102,** 56 (1980).
41. Feibelman, J., and Hamann, D. R., *Surf. Sci.* **149,** 48 (1985).